L_1 atomic-level width of elements $62 \leqslant Z \leqslant 83$

P.-A. Raboud, M. Berset, J.-Cl. Dousse, and Y.-P. Maillard
Department of Physics, University of Fribourg, Chemin du Musée 3, CH-1700 Fribourg, Switzerland
(Received 7 September 2001; published 17 January 2002)

High-resolution measurements of the photoinduced dipole-forbidden L_1-$M_{4,5}$ x-ray emission lines were performed with a reflection-type and a transmission-type bent-crystal spectrometer for $_{62}$Sm, $_{67}$Ho, $_{70}$Yb, $_{74}$W, $_{78}$Pt, $_{80}$Hg, and $_{83}$Bi. From the observed linewidths of the L_1-$M_{4,5}$ x-ray transitions, the level widths of the subshell L_1 were determined assuming for the $M_{4,5}$ level widths the values reported recently by Campbell and Papp [X-ray Spectrom. **24**, 307 (1995); At. Data Nucl. Data Tables **77**, 1 (2001)].

DOI: 10.1103/PhysRevA.65.022512 PACS number(s): 32.70.Jz, 32.30.Rj, 32.80.Fb

I. INTRODUCTION

Precise and reliable data concerning atomic-level widths are of interest in both theoretical and experimental physics. For theory such data are important because they can provide sensitive tests of atomic-structure calculations. In particular, they permit one to probe the goodness of theoretical predictions concerning total vacancy lifetimes, radiative and radiationless transition probabilities, or fluorescence yields. Atomic-level widths and related x-ray linewidths are also of interest and value in high-resolution x-ray spectroscopy. Here a precise knowledge of x-ray linewidths is very helpful because it permits one to improve data analysis by diminishing the number of free fitting parameters and anchoring the natural linewidths of the observed transitions to known values. This in turn leads to a better accuracy in x-ray emission techniques such as high-resolution x-ray fluorescence and particle-induced x-ray emission. Furthermore, in a variety of experiments in which weak structures such as radiative Auger emission lines or satellite x-rays have to be extracted from the tails of close-lying and much more intense diagram transitions, the line shapes of the latter must be known accurately to obtain reliable results.

Several review papers dealing with atomic-level widths can be found in the literature (see, e.g., [1–3]). Most rely on theory and only a few of them on experimental data. More recently Campbell and Papp assembled a large set of measured level widths and x-ray linewidths, and derived an internally consistent set of level widths for the K shell to the N_7 subshell for all elements across the periodic table [4,5].

For the subshell L_1 ($2s_{1/2}$ atomic level) Campbell and Papp used results from XPS (x-ray photoelectron spectroscopy) measurements for the light elements and XES (x-ray emission spectroscopy) data for the elements pertaining to the region $40 \leqslant Z \leqslant 51$. To connect the latter data to recent XES results obtained for Th and U [6,7], they chose to employ a set of L_1 Coster-Kronig and relative fluorescence yields of elements in the range $62 \leqslant Z \leqslant 79$ (Refs. [8–10]), assuming the radiative component of the L_1 widths, which was taken from [11]. The L_1 widths of Th and U were deduced by Campbell and Papp from the linewidths of the weak, dipole-forbidden L_1-M_4 and L_1-M_5 transitions observed in [6,7], assuming their recommended values for the M_4 and M_5 widths. The same references [6,7] provide also accurate linewidths for the stronger L_1-M_2, L_1-M_3, L_1-N_2, and L_1-N_3 lines but the latter were preferably employed as a source of the M_2, M_3, N_2, and N_3 widths, assuming the L_1 widths derived with the above-mentioned method. The alternative of using in the region $62 \leqslant Z \leqslant 79$ old XES measurements [12] of the L_1-$N_{2,3}$ linewidths instead of the set of L_1 Coster-Kronig yields was also probed by Campbell and Papp. The obtained results were found to be 0.3–3.3 eV higher than the values derived from Coster-Kronig spectroscopy. In their determination of the recommended L_1 widths, Campbell and Papp renounced to use these XES data because of the age of the latter, their Z dependence, and because of the 0.5–1.0 eV uncertainty in the $N_{2,3}$ widths. They pointed out, however, that there would be merit in remeasuring these L_1-$N_{2,3}$ transitions to ascertain if the trend determined from the Coster-Kronig spectroscopy data is indeed correct.

Following the suggestion of Campbell and Papp we have undertaken a series of high-resolution XES measurements in the Z region of interest. Although dipole-forbidden L_1-$M_{4,5}$ transitions are very weak, they were preferred to the stronger L_1-$N_{2,3}$ transitions because the uncertainties of the recommended $M_{4,5}$ widths quoted in [5] are two to ten times smaller than those of the $N_{2,3}$ widths and because it is not certain, in our opinion, that the many-body-effects, which considerably enlarge the widths of the $N_{2,3}$ levels in the domain comprised between Sn and Ba, are completely negligible for the elements $Z > 56$. Actually nonlifetime broadening effects seem to have been observed for these levels up to Yb ($Z = 70$) [13]. L_1-$M_{2,3}$ transitions could neither be employed because the single recent source of M_2 and M_3 level widths is the compilation by Campbell and Papp in which, the $M_{2,3}$ widths were already determined from L_1-$M_{2,3}$ transitions, assuming their recommended L_1 level widths. The quadrupole transitions L_1-$M_{4,5}$ of seven metallic elements in the range $62 \leqslant Z \leqslant 83$ were thus measured by means of high-resolution x-ray spectroscopy. From the observed linewidths, the level widths Γ_{L_1} were determined assuming for $\Gamma_{M_{4,5}}$ the recommended values of Campbell and Papp. Relative uncertainties varying between 4% (Bi) and 10% (Sm) were obtained for the so-derived L_1 level widths. Hence, a significant improvement of the existing Γ_{L_1} data base is given by the present study since the errors quoted in [5] for the same elements are 16% and 55%, respectively. A spin-off result of

our experiment is a set of accurate experimental energies for the weak L_1-M_4 and L_1-M_5 transitions.

II. EXPERIMENT

The measurements were performed at the University of Fribourg by means of two different curved-crystal spectrometers. For the elements $_{78}$Pt, $_{80}$Hg, and $_{83}$Bi a Dumond transmission-type crystal spectrometer was employed. As this instrument cannot be used for photon energies below about 10 keV, the L_1-M_4, and L_1-M_5 emission lines of the elements $_{62}$Sm, $_{67}$Ho, $_{70}$Yb, and $_{74}$W were measured with a von Hamos reflection-type crystal spectrometer.

Except for Hg, the targets consisted of 25-mm high $\times$5-mm wide metallic foils of natural Bi, Pt, W, Yb, Ho, and Sm. The specified purity of the foils ranged between 99.9% and 99.97%. Due to the method of production the Ho foil contained about 1% Ta. Bismuth being a brittle metal, the thin Bi foil was mounted on a permanent polyester support. Sample thicknesses (15–22 mg/cm^2) were chosen to obtain about 95% of the maximum possible yield. The liquid Hg was enclosed in a $(30\times8\times2)$-mm^3 stainless steel reservoir whose front wall was made of a 8-μm-thick Kapton foil. The small cell was oriented so that the angle between the normal to the Kapton window and the target-to-crystal direction was 45°.

A. Measurements of elements $78 \leqslant Z \leqslant 83$

A detailed description of a similar transmission-type bent-crystal spectrometer installed by the Fribourg group at the Paul Scherrer Institute (PSI) in Villigen, Switzerland can be found in [14]. The instrument was operated in a so-called modified DuMond slit geometry [14]. In this geometry the target is viewed by the bent crystal through a narrow slit located on the focal circle. The 0.1-mm-wide vertical rectangular slit was made of two 5-mm-thick juxtaposed Pb plates. The target L x-ray emission was induced by means of a commercial 3-kW Coolidge-type x-ray tube with a Cr anode and a 0.5-mm-thick window of nonporous beryllium. For the three targets the tube was operated at 80 kV and 35 mA. It was oriented so that the ionizing radiation was perpendicular to the target-crystal direction.

For the diffraction of the x rays the (110) reflecting planes of a 10×10-cm^2 quartz-crystal plate, 0.5 mm thick, were used. The quartz lamina was bent to a radius $R=313.5$ cm by means of a bending device similar to the one described in Ref. [15]. The effective reflecting area of the crystal was 12 cm^2. The Bragg angles, i.e., the angles between the incident x-ray radiation and the reflecting planes of the crystal were approximately 10.6°, 11.6°, and 12.4° for the Bi, Hg, and Pt target respectively. They were measured by means of an optical laser interferometer with a precision of $(3-5)\times10^{-3}$ arc sec [16].

The x-ray detector was a 5-in.-diameter two-component Phoswich scintillation counter, consisting of a thin (0.25 in.) NaI(Tl) crystal followed by an optically coupled thick (2 in.) CsI(Tl) crystal. Both crystals were mounted on the same photomultiplier tube. As the rising time of the signal is different for the two crystals, the events corresponding to each scintillation can be identified by pulse-shape analysis [17]. This type of detector strongly reduces the Compton noise arising from high-energy photons [7,18]. A further reduction of the background was achieved by enclosing the Phoswich detector in heavy Pb-Cu-Al shielding, and by sorting on line the events of interest as a function of their energy. In order to reduce the absorption of the x rays in air, evacuated tubes were mounted between the target and the crystal and between the crystal and the 66-cm-long Soller-slit collimator.

In the DuMond geometry, the measurements are carried out in a point-by-point way. As a result of the poor intensity of the L_1-$M_{4,5}$ transitions, very long acquisition times per point were needed. In order to minimize-systematic errors related to long-term instabilities of the experimental setup (e.g., fluctuations in the x-ray tube intensity), each spectrum was measured in many (30–40) successive scans, which were then summed off-line.

The energy calibration of angular spectra observed with the DuMond spectrometer requires the crystal lattice spacing and the zero of the Bragg-angle scale of the spectrometer to be accurately known. The lattice spacing of the SiO_2 (110) crystal employed in the present experiment was determined by measuring the $K\alpha_1$ transition of Au. The line was observed in fourth order of reflection and on both sides of reflection. Using the so-determined double Bragg angle $2\Theta_B$ and the energy of the Au $K\alpha_1$ transition (68804.94 $\pm$0.18 eV) quoted in [19], the value 2.456642(20) Å was obtained for the crystal lattice spacing. In the DuMond geometry the so-called focussing distance, i.e., the crystal-to-slit distance corresponding to the best instrumental resolution varies as a function of the photon energy. The L_1-$M_{4,5}$ measurements were thus performed at different focussing distances so that a new determination of the zero Bragg angle was necessary for each target. Because of the poor intensity of the L_1-$M_{4,5}$ transitions, stronger x-ray lines measured on both sides of reflection were employed for the determination of the different zero Bragg angles. These x-ray lines (Se $K\alpha_1$ and Hg $L\gamma_1$ in first order of reflection for the Pt and Hg measurements, and Te $K\alpha_1$ in second order of reflection for the Bi measurements) were chosen because they could be measured at about the same Bragg angle, i.e., at the same focussing distance as the L_1-$M_{4,5}$ transitions.

The instrumental response of the DuMond spectrometer can be well reproduced by a Gaussian function whose standard deviation σ depends mainly on the crystal quality, precision of the crystal curvature and slit width. In first approximation, the angular instrumental broadening does not depend on the Bragg angle, provided that the above-mentioned focusing distance is adjusted to correspond to the central Bragg angle of the measured spectrum. In other words, neglecting the contribution of the Darwin width, which is only a fraction of an arcsecond in our case, the angular resolution of the spectrometer can be considered as being the same for photons of different energies or photons diffracted in different orders of reflection. We took advantage of this property to determine the angular instrumental broadening of the spectrometer. The latter was indeed derived from the $K\alpha_1$ transition of Sn measured in first, second, and third orders of

reflection. From these measurements, we obtained a set of three equations with two unknowns, the angular instrumental broadening σ and the natural linewidth of the Sn $K\alpha_1$ transition Γ. Solving this set of equations by means of a nonlinear least-squares-fit method, we obtained $\sigma = 5.21 \pm 0.10$ arc sec and as a spin-off result, $\Gamma = 11.04 \pm 0.11$ eV. The latter result was found to be in good agreement with the value of 10.96 ± 0.38 eV derived from [5]. The obtained angular broadening of the spectrometer of 5.21 arc sec corresponded to FWHM (full width at half maximum) instrumental resolutions of 3.2, 3.6, and 4.4 eV, respectively, for the Pt, Hg, and Bi L_1-$M_{4,5}$ x-ray spectra.

B. Measurements of elements $62 \leqslant Z \leqslant 74$

The von Hamos curved crystal facility is described in detail in [20]. The principal elements of this instrument are an x-ray source defined by a rectangular slit, a cylindrically bent crystal, and a position-sensitive detector. In the von Hamos geometry the crystal is bent around an axis that is parallel to the direction of dispersion and provides focusing in the nondispersive direction. For a fixed position of the components, the impact coordinate on the detector of a reflected x-ray corresponds geometrically to a particular Bragg angle and hence to a particular photon energy. In contrast to the DuMond geometry, the von Hamos geometry permits thus at one position of the spectrometer components data collection over an energy bandwidth, which is limited by the detector length. The vertical rectangular slit consisted of two juxtaposed Ta pieces 0.3 mm thick and 10 mm high. The slit width was 0.1 mm for all measurements. The target L x-ray emission was also induced by means of a Cr anode x-ray tube. The latter was operated at lower high-voltage values (typically 60 kV, 40 mA).

Emitted photons were reflected in the first order by the $(2\bar{2}3)$ reflecting planes of a quartz crystal. The curvature radius of the 5-cm-wide and 10-cm-high crystal was 25.4 cm. Reflected photons were detected by a 27.6-mm-long and 6.9-mm-high deep-depleted (50 μm) CCD (charged-coupled device) position-sensitive detector. The latter, which consisted of 1024 pixels in the horizontal direction of dispersion and 256 pixels in the vertical direction, with a pixel resolution of 27 μm, was thermoelectrically cooled down to $-60\,^{\circ}$C. The diffracted x rays hitting the CCD built a two-dimensional pattern on the detector. Each measurement consisted in collecting several thousands of two-dimensional images. For each image, good event pixels were sorted by setting an energy window corresponding to the x rays of interest. This permitted us to reject background events and higher-order reflections. Without this sorting process, it would have been almost impossible to resolve the extremely weak L_1-$M_{4,5}$ transitions. The filtered images were then added and their sum projected on the horizontal axis to obtain the final energy spectrum.

The energy calibration and the determination of the instrumental response of the von Hamos spectrometer were performed by measuring the $K\alpha_1$ x-ray lines of several elements ranging between $26 \leqslant Z \leqslant 33$. It was found that for this energy range (6404–10 544 eV) the instrumental response of the spectrometer could be well reproduced by a Gaussian profile whose standard deviation σ varied as a function of the x-ray energy between 1.44 and 1.78 eV. The natural linewidths and energies of the $K\alpha_1$ transitions were taken from Ref. [5] and Ref. [21], respectively.

III. DATA ANALYSIS

The L_1-$M_{4,5}$ x-ray spectra observed with the DuMond and the von Hamos spectrometers were analyzed by means of the least-squares-fitting computer code MINUIT [22], employing Voigtian profiles to reproduce the observed x-ray lines. Voigtian functions were used because they correspond to the convolution of the Gaussian instrumental broadening with the Lorentzian representing the natural line shape of an x-ray transition. The natural widths of the x-ray lines of interest were extracted by keeping fixed in the fit the known Gaussian experimental broadening. The energies and the intensities of the transitions as well as a linear background were used as additional free fitting parameters. The fitted spectra are presented in Figs. 1 and 2.

At first glance, one sees that, as expected, the measured transitions are very weak, the net intensity at the top of the L_1-M_5 transitions varying from 0.07 s^{-1} for Bi [Fig. 1(a)] down to 0.003 s^{-1} for Sm [Fig. 2(d)]. These weak intensities originate from the poor x-ray emission rates of the L_1-$M_{4,5}$ transitions (for Sm, the yield ratio $I_{L_1\text{-}M_5}$:$I_{K\text{-}L_3}$ quoted by Scofield [23] is only 3×10^{-4}) and from the low efficiency of crystal spectrometers. This low efficiency, which is due mainly to the small solid angle subtended by crystal spectrometers (about 10^{-5} sr for both instruments in our case), is the price to pay to obtain instrumental resolutions in the eV range. The measured yield ratios $I_{L_1\text{-}M_4}$:$I_{L_1\text{-}M_5}$ were found to slightly decrease with Z, varying from 0.72 for Sm down to 0.62 for Bi. In this Z region, Scofield's calculations predict for this ratio a constant value of 0.67 [23]. In case of Yb, the fitted ratio is bigger than 1 (1.08). This is due to the L_3 absorption edge, which is located at 8944 eV, i.e., between the L_1-M_4 and L_1-M_5 transitions.

For transmission-type spectrometers, an additional factor that contributes to diminish the luminosity of the instrument is the x-ray absorption by the crystal lamina. For Pt, the lightest element that could be measured with the DuMond spectrometer, about 80% of the L_1-$M_{4,5}$ x-rays were absorbed in the 0.5-mm-thick quartz crystal so that about 16 days were needed to scan the single L_1-M_5 transition [Fig. 1(c)]. Thus, for this element, we renounced to measure the even weaker L_1-M_4 transition. Nevertheless, as shown in Fig. 1, in spite of this crystal absorption problem, clean data were obtained with the DuMond spectrometer. In the three spectra the lines of interest could be indeed clearly resolved from the relatively flat background and no particular problem was encountered during the analysis, which led to precise and reliable results.

For the lower-Z elements observed with the von Hamos spectrometer, the measurements and data analysis were complicated with the presence of several L_3 x rays in the vicinity of the L_1-$M_{4,5}$ lines of interest, namely, the L_3-$N_{6,7}$ and L_3-$O_{4,5}$ lines in the W spectrum [Fig. 2(a)], the L_3-O_1 and

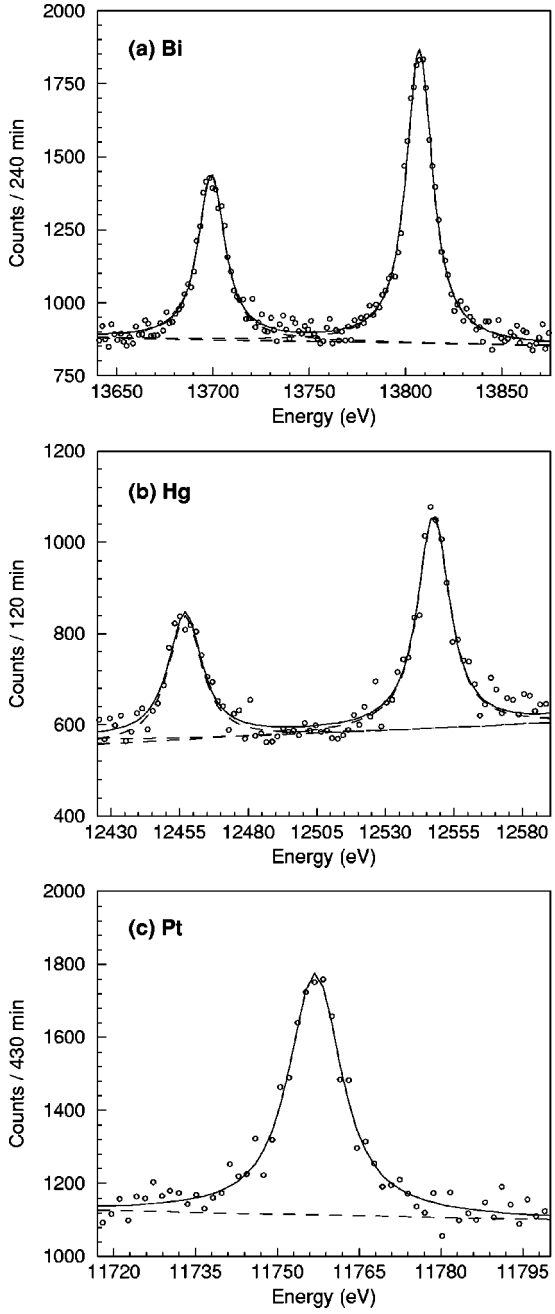

FIG. 1. High-resolution L_1-$M_{4,5}$ x-ray emission spectra measured with the DuMond transmission-type crystal spectrometer. For Pt, only the L_1-M_5 transition was measured.

L_3-$N_{6,7}$ lines in the Yb and Ho spectra [Figs. 2(b) and 2(c)], and the L_3-O_1 line in the Sm spectrum [Fig. 2(d)]. Some characteristic x ray lines from trace impurities in the targets or anode of the x ray tube were also observed in the W, Ho, and Sm spectra at energies of 10 275, 8086, and 6623 eV, respectively. Whereas a clear assignment was found for the first two lines (Re $L\beta_2$ and Ta $L\alpha_2$), the third one could not be identified undoubtedly. Furthermore, for Ho and especially Sm, the L_1-$M_{4,5}$ lines are sitting on the high-energy tail of the strong close-lying $L\beta_{2,15}$ doublet (L_3-$N_{4,5}$ transition). As the fitted values of the linewidth and intensity of the L_1-$M_{4,5}$ x-ray lines were found to be sensitive to the shape of the $L\beta_{2,15}$ tails, high-resolution measurements of the L_3-$N_{4,5}$ transition were performed for Ho and Sm. Results of these complementary measurements are shown in Fig. 3. One sees that for both targets the $L\beta_{2,15}$ lines are broad and evince strong asymmetries on their low-energy flank. This nonlifetime broadening is characteristic of rare-earth elements. It has been already observed [24,25] and explained in terms of multiplet splitting of the $4d_{3/2}$ and $4d_{5/2}$ orbitals as a result of exchange interactions between $4f$ and $4d$ electrons. In the fitting procedure, the asymmetric profiles of the Ho and Sm L_3-$N_{4,5}$ transitions could be well reproduced by the sum of, respectively, three and four Voigtians, whose position, Lorentzian width, and relative intensity were used as free fitting parameters. These parameters were then kept fixed at the obtained values in the analysis of the L_1-$M_{4,5}$ spectra, except the intensity of the strongest Voigtian, which was let free and served thus as a scaling factor.

A further complication encountered in the analysis of the spectra measured with the von Hamos spectrometer arose from satellite x-ray lines. Indeed, as a result of L_iL_jN and L_iL_jM Coster-Kronig transitions, L_2 and L_3 fluorescence x rays may present on their high-energy side *N*- and *M*-satellite structures of significant intensities. In general, the energy shifts of satellites relative to the parent diagram lines increase with the principal quantum number of the transition electron and decrease with the principal quantum number of the spectator vacancy. As a result, for *L* x rays, *M* satellites can be well resolved whereas *N* satellites are poorly separated from the diagram lines and occur only as asymmetries on the high-energy flank of the latter, except for transitions from the outer subshells O_i for which a better separation is observed. In addition, as the spectator vacancies can be located in different subshells and many couplings between the two holes are possible in the initial and final states, satellite lines consist of numerous components that vary in energy and intensity. Profiles of satellite x-ray lines are thus broad and the probability for satellites to overlap with other diagram lines is not negligible in *L* x-ray spectra. In measurements employing x-ray tubes for the production of the target fluorescence x ray emission, double $L^{-1}N^{-1}$ or $L^{-1}M^{-1}$ hole states can also be induced by *KLN* or *KLM* Auger transitions, provided that the high voltage of the x ray lamp is markedly bigger than the $1s$ binding energy of the irradiated target element. *KLM* Auger yields being smaller than *LLM* Coster-Kronig yields, only *M*-satellite structures related to strong *L* diagram lines have, however, to be considered in this case. For W, Yb, Ho, and Sm, L_iL_jM Coster-Kronig transitions are energetically forbidden and only the *K*-shell binding energy of Sm (48.6 keV) is significantly smaller than the high-voltage value (60 kV) at which the x-ray tube was operated. For this reason, the L_1-$M_{4,5}$ spectrum of Sm is the single one that might be affected by *M* satellites. Actually, the excess of intensity observed between the L_1-M_4 and L_1-M_5 lines [Fig. 2(d)] is due to the $L_3^{-1}M^{-1}$-$N_{4,5}^{-1}M^{-1}$ satellite transition. The latter was fitted with a single Lorentzian whose energy, width, and intensity were let free in the analysis. An energy shift of about 54 eV was obtained from the fit. This result was compared to values derived from the

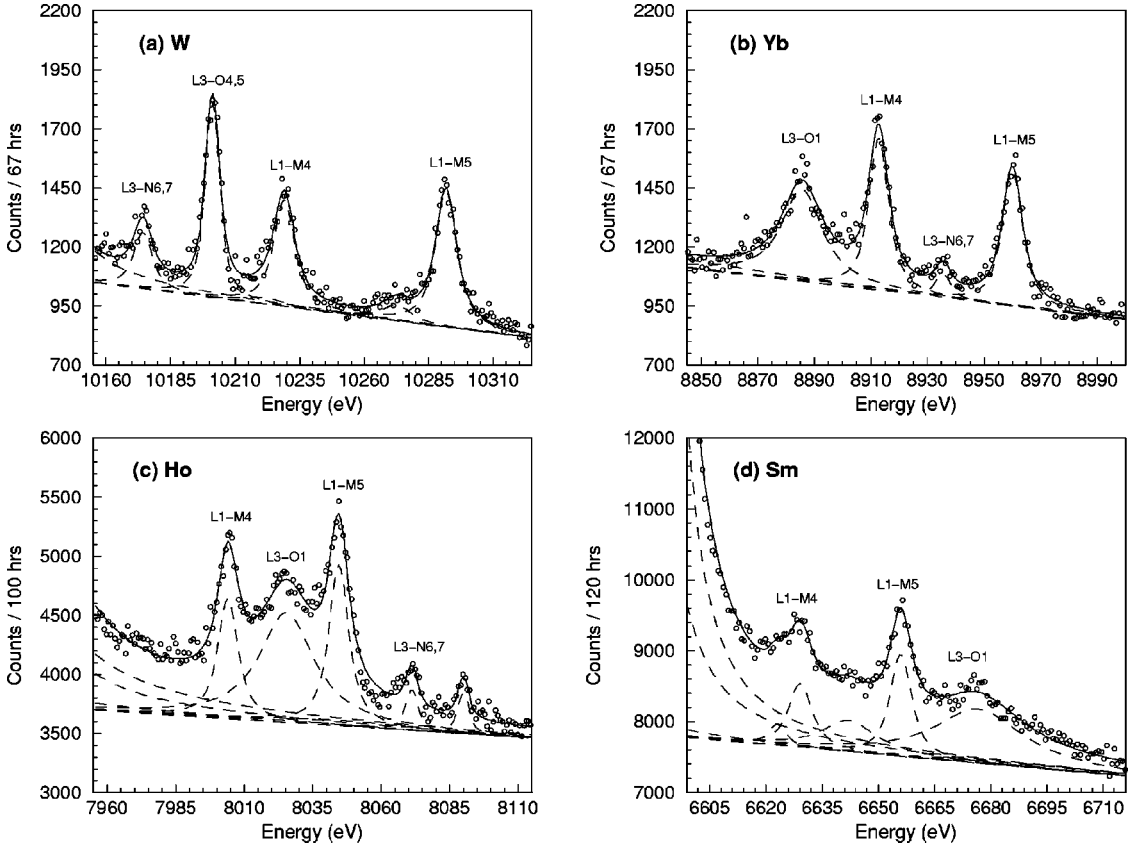

FIG. 2. High-resolution L x-ray emission spectra measured with the von Hamos reflection-type crystal spectrometer. The lines observed at 10 275 eV in the W spectrum and at 8086 eV in the Ho spectrum correspond to the Re $L\beta_2$ and Ta $L\alpha_2$ transitions from trace impurities in the targets and anode of the x-ray tube. In the Sm spectrum the broad line at about 6640 eV corresponds to the M satellite of the L_3-$N_{4,5}$ transition, whereas the excess of intensity occurring at 6623 eV could not be identified clearly. The intensity increases appearing on the low-energy sides of the Ho and Sm spectra are due to the tails of the strong L_3-$N_{4,5}$ transitions.

data quoted in [26,27]. A satisfactory agreement of the order of a few eV was found.

N satellites of the L_3-$O_{4,5}$ (W) and L_3-O_1 (Yb, Ho, and Sm) transitions were also included in the data analysis. As shown in Fig. 2(a), the N satellite (at about 10 220 eV) of the W L_3-$O_{4,5}$ transition is overlapping with the L_1-M_4 line. Any attempt to let free in the fit the satellite parameters failed so that the energy, Lorentzian width, and relative intensity of this satellite had to be kept at fixed values. The latter, however, could not be derived from Ref. [26] in which L-O transitions are not considered, neither from [27], which gives results for M satellites only. The difficulty was circumvented by measuring the L_3-$O_{4,5}$ transition of Hg with the DuMond spectrometer. Mercury was chosen because the $L_3^{-1}N^{-1}$-$O_{4,5}^{-1}N^{-1}$ satellite of this element was found to be well resolved from the diagram line and not overlapping with any other transition. The values obtained from the fit for the energy shift ΔE, width $\Gamma_{\rm sat}$, and relative intensity $I_{\rm sat}$:$I_{\rm diagr}$ of the Hg satellite were then employed to determine the unknown W N-satellite parameters. The dependence of the satellite parameters on the atomic number Z of the target element was taken into account by means of the following relations:

$$\Delta E(Z) = \Delta E(Z=80)[1+\alpha(Z-80)], \tag{1}$$

$$\frac{\Gamma_{\rm sat}}{\Gamma_{\rm diagr}}(Z) = \frac{\Gamma_{\rm sat}}{\Gamma_{\rm diagr}}(Z=80)[1+\alpha(Z-80)], \tag{2}$$

$$\frac{I_{\rm sat}}{I_{\rm diagr}}(Z) = \frac{I_{\rm sat}}{I_{\rm diagr}}(Z=80)\,\frac{\Sigma\Gamma_{LLN}(Z)}{\Sigma\Gamma_{LLN}(Z=80)}. \tag{3}$$

The Z-scaling factor α was deduced from the plots given in Ref. [27] for M satellites of L_1-$O_{2,3}$ transitions, assuming thus a similar dependence on Z for N and M satellites. The transition widths $\Gamma_{\rm diagr}$ were derived from the level widths quoted in [5] and the Coster Kronig yields Γ_{LLN} were taken from [28]. The same method was employed to determine the N-satellite parameters of the transitions L_3-O_1. The crudity of these approximations was taken into consideration by assuming relative uncertainties of 20% for the so-determined N-satellite parameters.

IV. RESULTS AND DISCUSSION

A. Energies

The energies of the measured L_1-$M_{4,5}$ transitions are given in Table I. For Pt, Hg, and Bi our results are based on the energy of the Au $K\alpha_1$ transition, which was determined by Kessler *et al.* with a precision of 2.6 ppm [19]. The un-

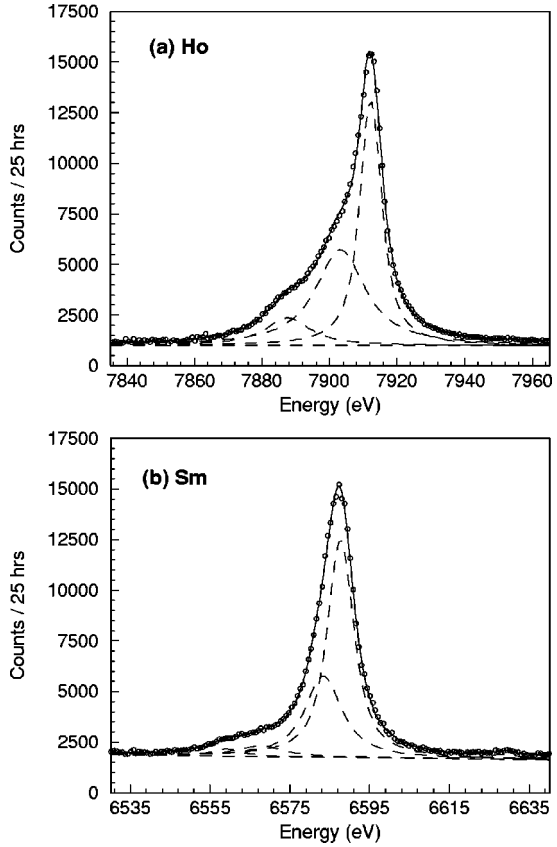

FIG. 3. High-resolution x-ray spectra of the $L\beta_{2,15}$ transitions of (a) holmium and (b) samarium.

certainties quoted for these three elements reflect mainly the statistical errors given by the fitting procedure. Uncertainties that originate from the crystal lattice spacing and from the determination of the zero Bragg angles are included in the indicated total errors. For Sm, Ho, Yb, and W, our values were determined from the $K\alpha_1$ wavelengths of Co, Cu, Zn, and As listed in the table of Bearden [21]. Since the latter values are given in the Å* scale, they were corrected by the conversion factor 1.000 016 7 Å/Å* [29] and then converted to energies using the energy-wavelength product $V\lambda = 12\,398.520$ eV Å [30]. The uncertainties quoted by Bearden [21] being probable errors (50% confidence limits), they were expanded by 1.48 to obtain standard deviation errors (67% confidence limits). The so-determined reference energies and associated errors are given as footnotes in Table I. Here again, statistical errors represent the principal source of uncertainty. The sensitivity of the L_1-$M_{4,5}$ transition energies to the fitted satellite structures was probed. The corresponding uncertainties were considered in the error budget. Further sources of uncertainties inherent to the von Hamos spectrometer such as the distance between the crystal and detector axes were also taken into account in the total errors.

To our knowledge there are no other high-resolution data concerning L_1-$M_{4,5}$ x rays in the domain $62 \leqslant Z \leqslant 83$. Hence, the present results were compared to values that were derived from the differences between the L_1 and M_4 or M_5 binding energies given by Bearden and Burr [31] and Storm and Israel [32]. From Table I one sees that deviations ranging from -3 to $+3$ eV are observed. One can also notice that most of Bearden and Burr's data, for which the quoted probable errors were converted in Table I to 1-σ errors as discussed above, are inconsistent with our results. Because modern data concerning core-level energies for the elements investigated in the present study are scarce, we are not in a position to discuss in detail the observed deviations. However, in case of Sm, the single studied element for which we found more recent data for the $M_{4,5}$ binding energies [33], values of 1110.9 and 1083.4 eV are given that are also in disagreement with the values of 1106.0 ± 0.8 and 1080.2 ± 0.6 eV quoted by Bearden and Burr. Furthermore, for the *N* subshells for which relatively modern information is available [34], similar deviations of 1–3 eV are observed relative to [31] for W, Pt, Hg, and Bi. For the N_3 level of Hg, the

TABLE I. Energies in eV of the measured L_1-$M_{4,5}$ x-ray emission lines. Present results are compared to the data of Bearden and Burr [31] and Storm and Israel [32].

	L_1-M_4					L_1-M_5				
		Error					Error			
Z	Energy	Fit	Total	Ref. [31]	Ref. [32]	Energy	Fit	Total	Ref. [31]	Ref. [32]
$_{62}$Sm	6 628.75[a]	0.21	0.26	6 630.8(1.3)	6 630	6 555.66[a]	0.13	0.14	6 656.6(1.2)	6 658
$_{67}$Ho	8 004.18[b]	0.14	0.15	8 002.7(1.2)	8 002	8 044.71[b]	0.13	0.14	8 042.8(1.3)	8 043
$_{70}$Yb	8 913.22[c]	0.12	0.14	8 910.1(9)	8 912	8 960.55[c]	0.18	0.19	8 958.6(9)	8 961
$_{74}$W	10 228.86[d]	0.20	0.24	10 228.2(6)	10 227	10 291.71[d]	0.17	0.22	10 290.6(6)	10 289
$_{78}$Pt						11 756.87[e]	0.20	0.22	11 758.3(7)	11 758
$_{80}$Hg	12 457.05[e]	0.51	0.52	12 454.4(1.5)	12 457	12 547.60[e]	0.26	0.29	12 544.4(1.5)	12 547
$_{83}$Bi	13 698.96[e]	0.30	0.32	13 699.9(7)	13 702	13 806.91[e]	0.16	0.20	13 807.9(7)	13 810

[a]Reference energy: 6930.44(5) eV (Co $K\alpha_1$).
[b]Reference energy: 8047.92(2) eV (Cu $K\alpha_1$).
[c]Reference energy: 8639.01(6) eV (Zn $K\alpha_1$).
[d]Reference energy: 10543.86(13) eV (As $K\alpha_1$).
[e]Reference energy: 68804.94(18) eV (Au $K\alpha_1$ $n=4$).

TABLE II. Natural linewidths in eV of the measured L_1-$M_{4,5}$ x-ray emission lines.

	L_1-M_4			L_1-M_5		
		Error			Error	
Z	Linewidth	Fit	Total	Linewidth	Fit	Total
$_{62}$Sm	5.94	0.68	0.76	5.53	0.56	0.62
$_{67}$Ho	7.45	0.60	0.61	7.31	0.42	0.44
$_{70}$Yb	6.60	0.38	0.40	6.91	0.38	0.40
$_{74}$W	7.96	0.60	0.65	8.21	0.50	0.52
$_{78}$Pt				10.63	0.66	0.66
$_{80}$Hg	13.39	1.39	1.39	12.75	0.93	0.93
$_{83}$Bi	15.27	0.79	0.79	15.00	0.47	0.47

deviation is even 5.6 eV, i.e., four times larger than the probable error given by Bearden and Burr for this level.

To better probe the precision and reliability of our results, we also measured the L_1-N_3, M_4-N_6, and M_5-N_7 transitions of Hg. For the first transition, which was observed with the DuMond spectrometer, an energy of $14\,266.16 \pm 0.22$ eV was obtained. By adding to the latter value the N_3 binding energy taken from [35] one finds a value of $14\,843.06 \pm 0.30$ eV for the binding energy of the L_1 level (the corresponding value quoted by Bearden and Burr is $14\,839.3 \pm 1.0$ eV). The M_4-N_6 and M_5-N_7 lines were measured with the von Hamos spectrometer. From the obtained transition energies (2282.25 ± 0.05 and 2195.57 ± 0.12 eV) and the $N_{6,7}$ binding energies given in [35], values of 2386.25 ± 0.11 and 2295.57 ± 0.16 eV were found for the binding energies of the M_4 and M_5 levels (Bearden and Burr give values of 2384.9 ± 0.3 and 2294.9 ± 0.3 eV, respectively). The energies of the L_1-$M_{4,5}$ transitions derived from the so-determined L_1 and $M_{4,5}$ binding energies are thus $12\,456.81 \pm 0.32$ and 12547.49 ± 0.34 eV, values which are both in good agreement with the Hg results presented in Table I.

B. Linewidths

The fitted linewidths of the L_1-$M_{4,5}$ transitions and the corresponding uncertainties are presented in Table II. As for the energies, the principal contribution to the total error originates from the matrix error of the fitting procedure. This is not really surprising in view of the poor intensity of the L_1-$M_{4,5}$ transitions. For Pt, Hg, and Bi, which were measured with the DuMond spectrometer, the natural linewidths are 3-4 times bigger than the instrumental broadening. As the latter could be determined with a precision of about 2%, the contribution of the instrumental response uncertainty to the total errors quoted in Table II is negligibly small.

As there is no existing information in the literature about measured linewidths of the weak L_1-$M_{4,5}$ transitions, we have compared our results to values derived from the sum of the L_1 and $M_{4,5}$ level widths quoted by Campbell and Papp [5]. The comparison showed that our data agree with the ones of Campbell and Papp within the total errors quoted in Table II, except for Ho and Sm for which a strong discrepancy is observed. For these two elements, our values are indeed about 1.6 eV bigger than those deduced from [5]. To better understand the origin of this disagreement, the L_2-M_4, L_1-M_2, and L_1-$N_{2,3}$ transitions of Ho as well as the L_1-$N_{2,3}$ transition of Sm were measured with the von Hamos spectrometer.

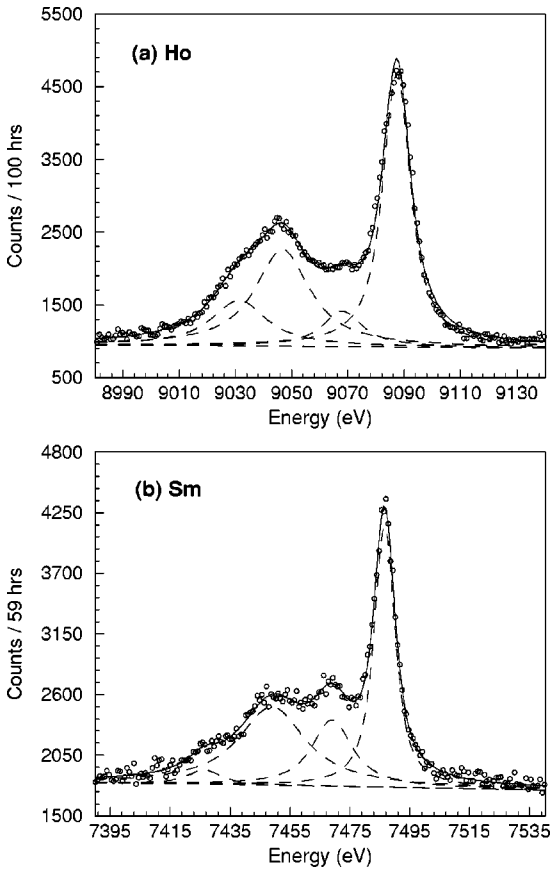

FIG. 4. High-resolution x-ray spectra of the $L\gamma_{2,3}$ transitions of (a) holmium and (b) samarium.

The L_2-M_4 and L_1-M_2 transitions that are close in energy could be measured simultaneously, the two transitions being covered by a single CCD length. The analysis of these two lines did not give rise to any problem. The $L\gamma_{2,3}$ x-ray lines (L_1-$N_{2,3}$ transitions) of Ho and Sm are presented in Fig. 4. For both elements a complex spectral profile was observed. Similar line shape were obtained in XES measurements of rare-earth-metal elements [36] and in $4p$ XPS measurements of elements ranging from $_{42}$Mo to $_{73}$Ta [13]. The observed anomalous features of the spectra were explained by the strong configuration interaction between $4f$ single-hole states and $4d$ double-hole states resulting from $4p^{-1}$-$4d^{-2}4(n,\epsilon)4f^{n+1}$ super-Coster-Kronig transitions. As shown in Fig. 4, the two complex $L\gamma_{2,3}$ profiles could be fitted with four juxtaposed Voigtians each. As reported in [38], for Sm, the main peak at 7486 eV should correspond to the well-defined relaxed core level of the $4p_{3/2}$ hole with more than half of the original strength peak of the $4p_{3/2}$ hole. Assuming the same interpretation for Ho, we also assigned the strongest Voigtian at 9087 eV to the L_1-N_3 transition.

TABLE III. Atomic-level widths in eV for the subshell L_1. Our experimental results are compared with the recommended values of Campbell and Papp [5] and theoretical predictions of Perkins *et al.* [11] and McGuire [37].

	Experimental		Theoretical		
Z	Present	Ref. [5]	Ref. [11]	Ref. [37]	
$_{62}$Sm	4.83±0.49	3.3±1.5	4.3		
$_{67}$Ho	6.23±0.36	4.5±1.5	5.0	5.1[a]	5.9[b]
$_{70}$Yb	5.40±0.30	5.2±1.5	8.0		
$_{74}$W	6.41±0.43	6.3±1.5	11.6	6.7[a]	7.8[b]
$_{78}$Pt	8.55±0.69	8.8±2.0	13.4		
$_{80}$Hg	10.67±0.79	10.5±2.0	13.8		
$_{83}$Bi	12.50±0.45	12.3±2.0	14.0	14.5[a]	19.3[b]

[a]Direct calculations.
[b]Adjusted calculations.

For the L_2-M_4 transition of Ho, a linewidth of 5.34 ±0.13 eV was obtained from the fit, in good agreement with the value of 5.22±0.42 eV deduced from [5]. For the L_1-M_2 and L_1-N_3 transitions, however, linewidths of 13.84±0.18 and 10.62±0.13 eV were found, results that are both bigger than the values of 10.8±1.7 and 7.5±1.6 eV derived from [5]. For Sm, the same trend was observed, the measured L_1-N_3 linewidth (7.05±0.18 eV) being bigger than the value (5.5±1.6 eV) deduced from the tables of Campbell and Papp. We are thus inclined to explain the discrepancies observed in the Ho and Sm transitions involving the L_1 subshell by a nonlifetime broadening of the 2*s* level. This effect will be discussed more in details in the following section.

C. Level widths

The L_1 level widths obtained in the present study are presented in Table III. They were determined from the weighted averages of the differences between the linewidths of the L_1-M_4 and L_1-M_5 transitions given in Table II and the recommended values of the $M_{4,5}$ level widths quoted by Campbell and Papp [5]. For Pt, the L_1 width was derived from the sole L_1-M_5 transition. The 10% uncertainties assumed in [5] for the $M_{4,5}$ level widths are included in the indicated errors. The latter vary from 4% for the heaviest measured element (Bi) up to 10% for the lightest one (Sm). Also reported in Table III are the L_1 level widths recommended by Campbell and Papp [5] with the corresponding errors and theoretical predictions based on the independent-particle model from two different sources. The first one is a work by Perkins *et al.* [11] whose results can be found in the Lawrence Livermore National Laboratory Evaluated Atomic Data Library. The second set of theoretical predictions is due to McGuire [37]. Here, however, results are available for Ho, W, and Bi only. For the three targets two values are given, which correspond to results of either direct calculations or calculations in which some theoretical parameters were anchored on existing experimental data. Our results are also presented graphically in Fig. 5, which gives an overview of existing information about the level width of the subshell L_1 in the range $50 \leqslant Z \leqslant 92$.

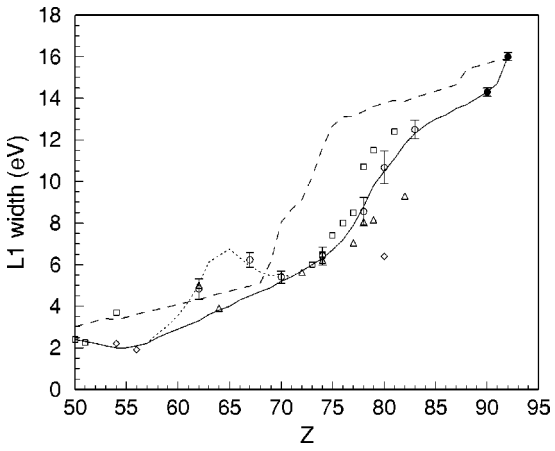

FIG. 5. Width L_1 versus atomic number *Z*. The solid line represents the recommended values of Campbell and Papp [5], the dashed line represents results of independent-particle model calculations of Perkins *et al.* [11], and the dotted line represents predictions derived from the present work for rare-earth-metal elements. Experimental data from different sources are also presented, using the following symbols: (◇) x-ray absorption edge results from Refs. [40,41], (△) results derived from Coster-Kronig transition probabilities from Refs. [8–10], (□) x-ray emission spectroscopy results from Refs. [12,39], (◆) x-ray emission spectroscopy results for thorium and uranium from Refs. [6,7], (○) present results.

As mentioned in the preceding section, an excellent agreement is found between our results and the values quoted in [5] for the elements $70 \leqslant Z \leqslant 83$, the average deviation (0.19 eV) being three times smaller than the average value of the quoted uncertainties (0.53 eV). In contrast to that, the results found for Ho and Sm are significantly bigger than the recommended values of Campbell and Papp. For Sm the deviation corresponds to about 3σ and for Ho even to 5σ, whereas for Yb, the third rare-earth-metal element investigated in the present study, no discrepancy is observed. At this point, it is interesting to note that for Sm a result of 5.0 ±0.6 eV, consistent with the value found in the present study, was obtained in a relatively recent Coster-Kronig measurement [8]. Some broadening of the L_1 subshell seems thus to affect Sm and Ho. Actually, a similar behavior is observed for the 5*s* level, the linewidths of the L_3-O_1 transition being about 10 eV broader for Sm and Ho than for Yb. However, the O_1 subshell broadening, contrary to the L_1 one, is not new. Indeed, a multiplet splitting of the 4*s* and 5*s* levels of the rare earth metals has been also observed in XPS measurements [42]. This splitting was explained to originate from the energy difference between the *s*-electron spin-up and spin-down final states. We are inclined to believe that the broadening of the L_1 level observed for Sm and Ho but not for Yb arises from the same effect. Assuming that the exchange interaction of the 2*s* hole in the initial state is larger or similar to the *LS* coupling energy of the 4*f* electrons, one can indeed consider the spin $s=\frac{1}{2}$ of the 2*s* subshell to couple with the spin *S* of the 4*f* subshell to yield the total

spin $S' = S \pm \frac{1}{2}$, so that the coupling results in a doublet. As the intensities of the two components of the doublet should be proportional to the respective multiplicities $(2S' + 1)(2L+1)$, the yield ratio of the two components is given by

$$\frac{I_1}{I_2} = \frac{[2(S+\frac{1}{2})+1](2L+1)}{[2(S-\frac{1}{2})+1](2L+1)} = \frac{S+1}{S}, \tag{4}$$

where I_1 stands for the intensity of the higher-energy component. The splitting energy can be deduced from Hartree-Fock calculations. A simpler process to describe the Z dependence of the broadening consists in assigning the two splitting components to the ''spin-up'' and ''spin-down'' $2s$ electrons. Neglecting the change in wave functions with Z, the splitting energy δE is then expected to be proportional to S and to the binding energy B_{L_1} of the $2s$ electron,

$$\delta E(Z) = \epsilon S(Z) B_{L_1}(Z). \tag{5}$$

For the trivalent-core Sm^{3+} ions embedded in the metal crystal, $S = 2.5$ so that the yield ratio $I_1 : I_2$ derived from Eq. (4) should be equal to 1.40. To determine the splitting coefficient ϵ, we refitted the Sm L_1-M_5 transition with two components. The width of the two Lorentzians was fixed at the value of 4.16 eV derived from the level widths given by Campbell and Papp and the intensity ratio at the above-mentioned value of 1.40. From the fit, a splitting $\delta E = 2.54 \pm 0.38$ eV was obtained, which led to $\epsilon = 1.31(20) \times 10^{-4}$. The one- and two-component fits of the L_1-M_5 transition of Sm are depicted in Fig. 6. For clarity the tails of the L_3-$N_{4,5}$ line, the L_1-M_4 and L_3-O_1 lines, as well as the N satellite of the latter and the background were subtracted beforehand from the measured L_1-$M_{4,5}$ spectrum. Approximately equal chi squares were found for the one-and the two-component fits.

To probe the goodness of the splitting model, we have compared the fitted linewidths of the L_1-M_5 transitions of Ho and Yb with the FWHM widths of theoretical profiles obtained from the sum of two Lorentzians of equal width. The latter was derived from [5] whereas the energy difference and intensity ratio of the two Lorentzians were determined from Eqs. (4) and (5), using for ϵ the value deduced from the two-component fit of Sm. Energy splittings of 2.47(37) and 0.69(10) eV and intensity ratios of 1.5 and 3.0 were found for Ho $(S=2)$ and Yb $(S=\frac{1}{2})$. The resulting FWHM widths of the corresponding theoretical profiles were found to be 7.09 ± 0.39 and 6.86 ± 0.09 eV, respectively, both results in a fair agreement with the L_1-M_5 linewidths presented in Table II. Applying the same method to the other rare-earth-metal elements and subtracting from the obtained theoretical linewidths the $M_{4,5}$ level widths quoted in [5], we were able to determine a new set of L_1 widths for the lanthanides region. Furthermore, as the parameter ϵ was deduced from the sole L_1-M_5 transition of Sm, the function $\Gamma_{L_1} = f(Z)$ was scaled by means of a least-squares-fit method

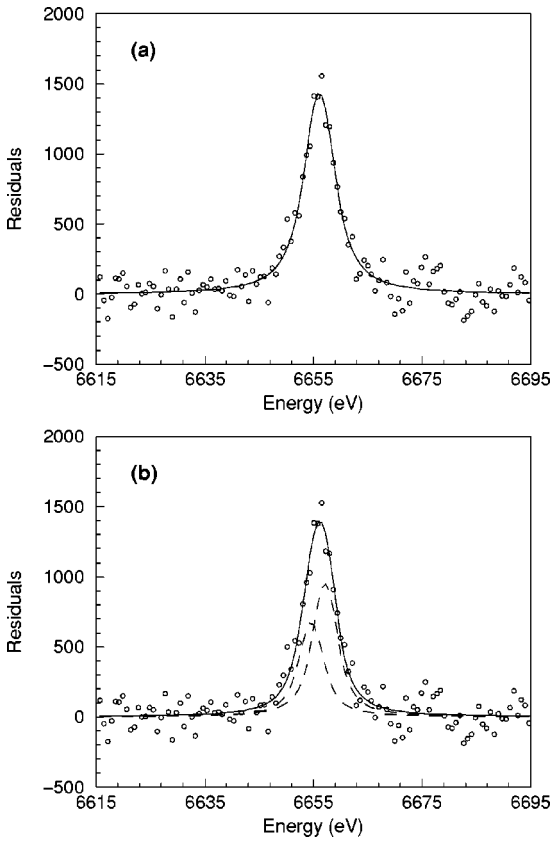

FIG. 6. One- and two-component fits of the residual L_1-M_5 x-ray spectrum of Sm.

to match the widths of Sm, Ho, and Yb quoted in Table III. The proposed new values are presented in Fig. 5 (dotted line).

As shown in Table III, our experimental L_1 level widths are, in general, smaller than the corresponding theoretical predictions. The reason for the discrepancy resides mainly in the theoretical Coster-Kronig yields, which are in most cases overestimated by the calculations. For Sm and Ho, an opposite trend is observed but this is due to the above-mentioned broadening of the L_1 level in rare-earth-metal elements, which is not considered in the calculations. Finally, subtracting the L_1 widths obtained in the present work from the observed linewidths of the L_1-N_3 transition of Sm and L_1-M_2 and L_1-N_3 transitions of Ho reported in the preceding section, values of 2.22(52) and 4.39(38) eV are found for the N_3 level widths of Sm and Ho and 7.61(40) eV for the M_2 level width of Ho. The corresponding widths quoted by Campbell and Papp are 2.2(5), 2.95(50), and 6.3(7) eV. A good agreement is thus observed for the N_3 level of Sm whereas differences of about 1.3 eV are found for both the N_3 and M_2 level widths of Ho.

V. CONCLUDING REMARKS

High-resolution measurements of the L_1-$M_{4,5}$ fluorescence x-ray lines of Bi, Hg, Pt, W, Yb, Ho, and Sm were performed. Despite the poor intensity of the dipole-forbidden transitions, precise energies and linewidths were obtained. A

comparison of the present experimental energies with differences between the binding energies of atomic levels listed by Bearden and Burr has shown that the latter binding energies have to be considered with precaution, deviations of several eV, i.e., larger than the quoted uncertainties being frequently observed.

Assuming for the $M_{4,5}$ level widths the values reported recently by Campbell and Papp, the L_1 level widths of the seven elements could be determined with a precision of 4–10 %. Whereas an excellent agreement with Campbell and Papp's data was observed for the five heaviest elements, an intriguing discrepancy was found for Ho and Sm. The observed deviations were explained by a splitting effect of the L_1 subshell resulting from the coupling of the $2s$ electron spin in the initial excited state with the total spin of the open $4f$ level. Based on this splitting picture, adjustments of the L_1 level widths recommended by Campbell and Papp were proposed for the lanthanides region. As in their work Campbell and Papp have determined the M_2 and M_3 level widths from XES measurements of the L_1-$M_{2,3}$ transitions, assuming their recommended L_1 level widths, the $M_{2,3}$ level widths they proposed for the rare-earth metals might be overestimated. Finally, in our opinion, a similar splitting effect should affect the width of the M_1 subshell of lanthanides. This point could be clarified by high-resolution measurements of the L_3-M_1 transitions of rare-earth metals. Such measurements are in progress at our laboratory.

ACKNOWLEDGMENT

This work was partly supported by the Swiss National Science Foundation.

[1] O. Keski-Rahkonen and M. O. Krause, At. Data Nucl. Data Tables **14**, 139 (1974).
[2] S. I. Salem and P. L. Lee, At. Data Nucl. Data Tables **18**, 234 (1976).
[3] M. O. Krause and J. H. Oliver, J. Phys. Chem. Ref. Data **8**, 329 (1979).
[4] J. L. Campbell and T. Papp, X-Ray Spectrom. **24**, 307 (1995).
[5] J. L. Campbell and T. Papp, At. Data Nucl. Data Tables **77**, 1 (2001).
[6] P.-A. Raboud, J.-Cl. Dousse, J. Hoszowska, and I. Savoy, Phys. Rev. A **61**, 012507 (2000).
[7] J. Hoszowska, J.-Cl. Dousse, and Ch. Rhême, Phys. Rev. A **50**, 123 (1994).
[8] R. Stötzel, U. Werner, M. Sarkar, and W. Jitschin, J. Phys. B **25**, 2295 (1992).
[9] T. Papp, J. L. Campbell, and S. Raman, Phys. Rev. A **58**, 3537 (1998).
[10] U. Werner and W. Jitschin, Phys. Rev. A **38**, 4009 (1988).
[11] S. T. Perkins, D. E. Cullen, M.-H. Chen, J. H. Hubbell, J. Rathkopf, and J. H. Scofield, Lawrence Livermore National Laboratory Report No. UCRL-50400, 1991 (unpublished).
[12] J. N. Cooper, Phys. Rev. **65**, 155 (1944).
[13] S. P. Kowalczyk, L. Ley, R. L. Martin, F. R. McFeely, and D. A. Shirley, Faraday Discuss. Chem. Soc. **60**, 7 (1975).
[14] B. Perny *et al.*, Nucl. Instrum. Methods Phys. Res. A **267**, 120 (1988).
[15] W. Beer, P. F. A. Goudsmit, and L. Knecht, Nucl. Instrum. Methods Phys. Res. A **219**, 322 (1984).
[16] W. Schwitz, Nucl. Instrum. Methods **154**, 95 (1978).
[17] R. C. Sharma *et al.*, Nucl. Instrum. Methods **130**, 305 (1975).
[18] Ch. Herren and J.-Cl. Dousse, Phys. Rev. A **53**, 717 (1996).
[19] E. G. Kessler, Jr., R. D. Deslattes, D. Girard, W. Schwitz, L. Jacobs, and O. Renner, Phys. Rev. A **26**, 2696 (1982).
[20] J. Hoszowska, J.-Cl. Dousse, J. Kern, and Ch. Rhême, Nucl. Instrum. Methods Phys. Res. A **376**, 129 (1996).
[21] J. A. Bearden, Rev. Mod. Phys. **39**, 78 (1967).
[22] F. James and M. Roos, Comput. Phys. Commun. **10**, 343 (1975).
[23] J. H. Scofield, At. Data Nucl. Data Tables **14**, 121 (1974).
[24] S. I. Salem, C. W. Schultz, B. A. Rabbani, and R. T. Tsutsui, Phys. Rev. Lett. **27**, 477 (1971).
[25] S. I. Salem and B. L. Scott, Phys. Rev. A **9**, 690 (1974).
[26] F. Parente, M. H. Chen, B. Crasemann, and H. Mark, At. Data Nucl. Data Tables **26**, 383 (1981).
[27] W. Uchai, C. W. Nestor, Jr., S. Raman, and C. R. Vane, At. Data Nucl. Data Tables **34**, 201 (1986).
[28] M. H. Chen, B. Crasemann, and H. Mark, At. Data Nucl. Data Tables **24**, 13 (1979).
[29] E. G. Kessler, Jr., R. D. Deslattes, and A. Henins, Phys. Rev. A **19**, 215 (1979).
[30] E. R. Cohen and B. N. Taylor, J. Phys. Chem. Ref. Data **2**, 663 (1973).
[31] J. A. Bearden and A. F. Burr, Rev. Mod. Phys. **39**, 125 (1967).
[32] E. Storm and H. I. Israel, Nucl. Data, Sect. A **7**, 565 (1970).
[33] G. Williams, http://xray.uu.se/hypertext/EbindEnergies.html
[34] J. C. Fuggle and N. Mårtensson, J. Electron Spectrosc. Relat. Phenom. **21**, 275 (1980).
[35] S. Svensson *et al.*, J. Electron Spectrosc. Relat. Phenom. **9**, 51 (1976).
[36] B. D. Shrivastava, R. K. Jain, A. Mishra, and Devendra Singh, J. Phys. B **19**, 3839 (1986).
[37] E. J. McGuire, Phys. Rev. A **3**, 587 (1971).
[38] M. Ohno and R. E. LaVilla, Phys. Rev. B **39**, 8852 (1989).
[39] M. Ohno and R. E. LaVilla, Phys. Rev. A **45**, 4713 (1992).
[40] I. Arcon, A. Kodre, M. Štuhec, D. Glavič-Cindro, and W. Drube, Phys. Rev. A **51**, 147 (1995).
[41] O. Keshki-Rahkonen, G. Materlik, B. Sonntag, and J. Tulkki, J. Phys. B **17**, L121 (1984).
[42] R. L. Cohen, G. K. Werthein, A. Rosencwaig, and H. J. Guggenheim, Phys. Rev. B **5**, 1037 (1972).